IEEE Access
Multidisciplinary ⋮ Rapid Review ⋮ Open Access Journal

Received 22 July 2022, accepted 5 August 2022, date of publication 8 August 2022, date of current version 15 August 2022.

Digital Object Identifier 10.1109/ACCESS.2022.3197631

APPLIED RESEARCH

Modeling and Design of Cookware for Induction Heating Technology With Balanced Electromagnetic and Thermal Characteristics

EMILIO PLUMED[1], (Member, IEEE), IGNACIO LOPE[1,2], (Member, IEEE), AND JESÚS ACERO[3], (Senior Member, IEEE)

[1]B/S/H/ Home Appliances, 50016 Zaragoza, Spain
[2]Department of Applied Physics, University of Zaragoza, 50009 Zaragoza, Spain
[3]Department of Electronic Engineering and Communications, I3A, Universidad de Zaragoza, 50018 Zaragoza, Spain

Corresponding author: Jesús Acero (jacero@unizar.es)

This work was supported in part by the Spanish MICINN and AEI under Project PID2019-103939RB-I00 and Project PDC2021-120898-I00, in part by EU through FEDER and NextGenerationEU/PRTR Programs, in part by DGA-FSE, and in part by the BSH Home Appliances Group.

ABSTRACT Improving the cooking experience of induction-heating users involves, among other factors, an optimized power distribution at the bottom of the cooking vessel. Conventional ferromagnetic cookware presents high efficiency but unequal temperature distribution with flat inductors, which subsequently leads to uneven cooking results. In this work, we propose an alternative to the traditional cookware arrangement by inserting some aluminum pieces in the ferromagnetic bottom of cookware. This arrangement combines the optimal inductive performance of the ferromagnetic iron an the high thermal conductivity of aluminum. The performance of the proposed arrangement is analyzed by means of a multiphysics tool including electromagnetic and heat transfer sub-models which is applied to predict both the equivalent electrical circuit and the temperature distribution in cookware. As a result, a balanced trade-off between efficiency and temperature distribution is evidenced with the proposed solution. Experimental results also corroborates the predictions of the proposed solution.

INDEX TERMS Induction heating, electromagnetic induction, finite element multiphysic simulation, magnetic devices.

I. INTRODUCTION

Induction heating (IH) has become the technology of choice for cooking due to its inherent advantages over other heat sources such as flames, resistances, microwaves or traditional ovens. Induction cookers are perceived by users as top range appliances, which offer attractive features such as cleanness, safety, high efficiency or automatic cookware detection. Part of these advantages derive from the fact that in IH cookers energy is wirelessly transferred into the pot and, consequently, the wasted energy is minimized. Other advantages derive from the advanced power electronics and user interface devices incorporated in commercial appliances [1].

The associate editor coordinating the review of this manuscript and approving it for publication was Giovanni Pau.

Basically, an induction burner consists of a planar coil supplied by an alternating current source. The current generates an alternating magnetic field which transfers energy towards the workpiece by means of the electromagnetic induction phenomenon. Part of the transferred energy can be harnessed for cooking purposes, as is schematically shown in Fig. 1.

IH cookers involve several enabling technologies as electromagnetic design, power electronics, digital control and heat transfer. In the last years, intense research efforts have been carried out about the design and fabrication of IH cookers with improved performance. This research was mainly focused on the mentioned key enabling technologies. Regarding electromagnetics, research activities ranges from inductors optimization [2], [3] to electromagnetic compatibility [4], [5]. Advances in power electronics include resonant

This work is licensed under a Creative Commons Attribution 4.0 License. For more information, see https://creativecommons.org/licenses/by/4.0/

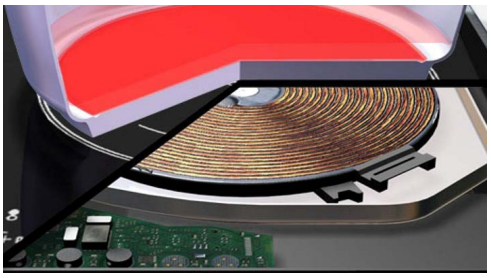

FIGURE 1. Representation of a domestic induction system consisting of a planar coil and the cookware.

inverters with improved performance or increased flexibility of use [6], [7]. Machine learning techniques are also being currently applied to automatic pot recognition [8], [9], whereas inverse models were proposed to predict the cookware temperature [10] from the electromagnetic energy profile. These works mainly consider the different enabling technologies separately. However, holistic approaches involving the above mentioned fields are essential for further advances in the IH technology [11].

Simulation of IH processes requires the ability to simultaneously model multiple coupled physics. It is necessary to account for the temperature dependent material parameters such as thermal properties (*e.g.* conductivity, specific heat) and electrical properties (*e.g.* resistivity, permeability) [12]. Finite Element (FE) analysis is the preferred tool to simulate IH applications due to its versatility and multiphysics analysis capability [13].

Many works dealing with electro-thermal simulations have been reported in the literature, mainly focused on industrial induction heating applications with solenoidal coils [14], [15], [16] or other eddy-current-based applications [17], [18], [19]. Other works propose tools for obtaining the temperature evolution in heat treatments, and also predict the stresses [20], [21] in order to optimize the heat processing. These proposed simulation strategies are also of interest for domestic induction heating systems. However, industrial and domestic applications have different geometries, power and temperature ranges, and objectives [22]. Specifically, in domestic applications the interest is focused on the efficiency of the energy conversion and the uniformity of the cooking results, which is translated into environmental benefits and user's cooking experience improvements.

Cooking results not only depends on the user ability but also on the temperature profile generated in the cookware by the induced eddy currents and its thermal behavior. In general little attention has been paid to aspects such as temperature profile or cooking results. There are two main ways to improve the temperature uniformity in the bottom of the cookware when using induction heating technology. First, the profile of the generated magnetic field in planar coils is determined in some extent by the position of the turns. Some design solutions, as unequally spaced turn coils, have been patented in order to achieve a more uniform temperature profile [23], [24], [25]. Moreover, other inductor arrangements based on Halbach's coils have also been proposed [26]. However these solutions require specific plastic housings to guide the turns, which increases the cost and engineering complexity. In general, coil arrangements with continuous turns are preferred by manufacturers due to their specific advantages, as cost savings, and easy of manufacturing. Regarding the cookware design, approaches to improve the temperature profile are not available in the current literature. In this work, the influence of the cookware structure on the uniformity of heating and efficiency is studied and the combination of two different materials is proposed.

For this purpose, a multiphysics finite element (FE) simulations is used in combination with experimental results. An electromagnetic solver was used to simulate the electric and magnetic varying fields. Moreover, the thermal energy transference governed by conduction, convection and radiation phenomena was simulated by means of a heat transfer solver. Due to the associated time-scales being very different, the electromagnetic solver provides a steady-state time harmonic solution which is coupled with the transient thermal analysis. Simulation results are tested under working conditions by means of specifically designed configurable loads and an infrared camera.

The paper is organized as follows. Section II presents the electromagnetic and heat-transfer analyses. An arrangement aimed to improve the temperature profile at the bottom of the cookware is proposed in Section III. In Section IV the experimental validation is presented and, finally, Section V summarizes the findings and conclusions of this work.

II. ELECTROMAGNETIC AND THERMAL ANALYSIS AND MODELING

A. THEORETICAL FOUNDATIONS

The electromagnetic part of the IH system is governed by Maxwell's equations, which determine the dependency of fields with respect to free charges and currents. Considering an impressed current density $\mathbf{J}_{coil}$ and disregarding free charge densities, the fields can be represented by means of the magnetic vector potential $\mathbf{A}$. This representation also requires to choose a gauge in order to cancel redundant degrees of freedom in fields. In this case the so called Coulomb's gauge ($\nabla \cdot \mathbf{A} = 0$) is adopted. In the harmonic formulation the vector potential satisfies the following diffusion equation:

$$\nabla^2 \mathbf{A} - j\omega\sigma_e \mathbf{A} = -\mu \mathbf{J}_{coil}, \tag{1}$$

where the harmonic dependence $e^{j\omega t}$ has been omitted for the sake of simplicity. Moreover, σ_e and μ are the electrical conductivity and magnetic permeability of materials, respectively. In this equation radiative effects have been neglected because the wavelengths of the fields are much larger than the characteristic size of typical systems. This equation is solved by means of the FE method.

Electric $\mathbf{E}$ and magnetic $\mathbf{H}$ fields are involved in magnitudes as dissipated power density, power factor, equivalent impedance and efficiency. These fields can be straightforwardly obtained from the vector potential

as follows:

$$\mathbf{E} = -j\omega\mathbf{A},$$
$$\mathbf{H} = \frac{1}{\mu} \cdot \nabla \times \mathbf{A}. \tag{2}$$

Poynting's vector $\mathbf{S}$ represents the electromagnetic energy density flowing through a surface. This magnitude is obtained from the $\mathbf{E}$ and $\mathbf{H}$ fields:

$$\mathbf{S} = \left(\mathbf{E} \times \mathbf{H}^*\right), \tag{3}$$

where $\mathbf{H}^*$ is the conjugate of the magnetic field. At harmonic regime, the real part of Poynting's vector flux corresponds to the power through a surface:

$$\dot{Q} = Re\left[\int_S \left[\left(\mathbf{E} \times \mathbf{H}^*\right) \cdot \hat{\mathbf{n}}\right] dS\right]. \tag{4}$$

where $\hat{\mathbf{n}}$ is the normal vector to the interest surface. $\dot{Q}$ is the magnitude required to couple the electromagnetic and heat transfer analysis.

Considering the temperature distribution resulting from the induction, the transient heat conduction equation is:

$$\rho c \frac{\partial T}{\partial t} + \nabla(-\lambda \nabla T) = \dot{Q}, \tag{5}$$

where T is the temperature, ρ is the density, c is the specific heat capacity, λ is the thermal conductivity and $\dot{Q}$ is the heat source from Eq. (4). At the interest temperature range for cooking, the thermal conductivity is assumed not to vary as a function of temperature.

Regarding the heat conduction simulation, boundary conditions are also needed. These conditions can be simply a prescribed temperature on the boundary and/or an imposed temperature flux in the surface. In this case, the last one is applied considering a radiation and convection boundary condition:

$$q_n = h(T_s - T_a) + \hat{\sigma}\hat{\varepsilon}(T_a^4 - T_s^4), \tag{6}$$

where q_n is related to the gradient of the temperature field in the normal direction of the surface ($\boldsymbol{n}$), i.e. $\frac{\partial T}{\partial \boldsymbol{n}}$, h is the convection surface heat transfer coefficient, T_s is the surface temperature, T_a is the ambient temperature, $\hat{\sigma}$ is the Stefan Boltzmann constant and $\hat{\varepsilon}$ is the emissivity of the surface.

B. COMPUTATIONAL MODELS

In this section, the expressions above described are adapted to the finite element simulation tools.

The commercial FE tool COMSOL Multiphysics was used for simulating the coupled electromagnetic and heat transfer phenomena of this system. This tool provides multiphysics simulation capability which is convenient to analyze the considered system.

Fig. 2 shows a schematic representation of the electromagnetic model of a domestic induction heating system including some representative parameters. This system comprises a planar coil, the glass-ceramic cooking surface, the workpiece to be heated, and a sheet of a aluminum placed below the other elements with the purpose of shielding the electronics or other objects from the magnetic field. Moreover, between the windings and shielding some ferrite bars are placed to increase the coupling with the pot. In order to achieve high inductive efficiency, the diameter of the cookware should be of the same size or greater than the coil diameter.

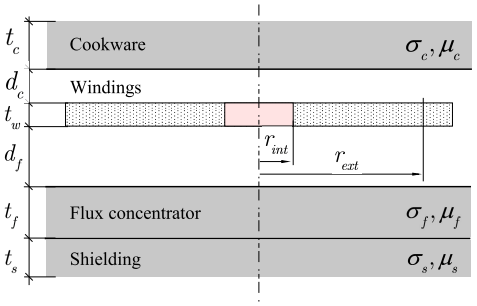

FIGURE 2. Schematic representation of the system under study with magnitudes involved in the electromagnetic model.

Basically, the planar coil consists of a spiral of n turns of a multistranded wire, also called *litz wire* [27]. Litz wires are multi stranded cables mainly used at medium-high frequency electrical applications in order to alleviate the ac losses due to *skin* and *proximity* effects. Litz wires are arranged by means of n_s isolated fine strands of diameter ϕ_s, which are twisted or braided together and connected in parallel [28]. Usually the dimensions of the coil are represented by means of the internal and external radius r_{int} and r_{ext}, and the coil thickness t_w, respectively.

The multi-turn spiral winding with the intricate litz wire structure was modeled as an ideal current density of rectangular cross section. This current density represents the external source required to solve (1). The current density is constant, frequency independent and in a cylindrical coordinate system is defined as follows:

$$\mathbf{J}_{coil} = \frac{I_{coil}}{S_{turn}}\hat{\boldsymbol{\varphi}} = n\frac{I_{coil}}{S_{coil}}\hat{\boldsymbol{\varphi}} = n\frac{I_{coil}}{t_w\left(r_{ext} - r_{int}\right)}\hat{\boldsymbol{\varphi}}, \tag{7}$$

where the harmonic dependence of the fields is included in the coil current $I_{coil} = \hat{I}_{coil}e^{j\omega t}$, with ω being the angular frequency. Moreover, S_{turn}, S_{coil} are the turn and the coil cross-sectional areas, respectively. It is convenient to remark that this ideal coils model doesn't capture the ohmic losses of windings. Considering that typical induction systems have high axial symmetry, sectors can be simulated instead of the whole system and thus saving computation time. In this case a quarter of the system was simulated. Electromagnetic simulation of sectors does not require additional boundary conditions because magnetic fields are parallel to the boundaries of the simulated sector. Moreover, an external domain combined with an infinite element domain is also included in the model with the purpose of properly simulating the fact that the fields are null at an infinite distance. Additionally, the Impedance Boundary Condition (IBC) is also used because it allows replacing a domain by equivalent boundaries when the skin depth of the fields at the frequency range of interest is

smaller than the thickness of the domain. This feature can be applied when the electromagnetic field decays quickly in the boundary, as occurs in good conductors at the interest working frequencies. According to this condition the equation (1) in the cookware can be simplified as follows:

$$\nabla^2 \mathbf{A} \cong \partial_z^2 \mathbf{A} = -j\omega\mu\sigma \mathbf{A}. \tag{8}$$

The IBC condition is appropriate to reduce the number of elements of the mesh and therefore is also appropriate to achieve computational savings. In this case the mesh consisted of 1.566.288 nodes and 230.000 tetrahedral elements. The solver was configured to carry out frequency domain simulations.

The equivalent impedance of an induction system is defined as the ratio of the voltage in the coil with respect to the current, $Z_{eq} = V_{coil}/I_{coil}$. The voltage is obtained by integrating the electrical field over the entire coil volume divided by the cross sectional area S_{coil} and multiplied by the number of turns n:

$$V_{coil} = -\oint_{windings} \mathbf{E} \cdot \mathbf{dl} = -\frac{n}{S_{coil}} \int_{r_{int}}^{r_{ext}} \int_0^{t_w} 2\pi r E_\varphi dz dr. \tag{9}$$

In general, Z_{eq} is complex and therefore it has real and imaginary parts. The real part represents power dissipation whereas the imaginary part represents the equivalent inductance of the system:

$$Z_{eq} = R_{eq} + j\omega L_{eq}. \tag{10}$$

According to the ideal current density model of the coil, the resistance R_{eq} only accounts for the power dissipated in the cookware and the power dissipated in the shielding. Let R_p, R_{sh} and R_w be the resistances representing the losses in the cookware, shielding and windings, respectively. Therefore:

$$R_{eq} = R_p + R_{sh}. \tag{11}$$

Consequently, the electrical power factor is:

$$PF = \frac{R_{eq}}{\sqrt{R_{eq}^2 + \left(\omega L_{eq}\right)^2}}. \tag{12}$$

The inductive efficiency represents the power delivered in the load with respect to the total electrical power supplied to the windings [27]. According to the FE model presented, R_{eq} only represents the power dissipated in the workpiece and the shielding, due to the adopted ideal model of windings. According to the definition of R_{eq}, the inductive efficiency of the domestic IH system is defined as follows:

$$\eta_{ind} = \frac{R_p}{R_{eq} + R_w} = \frac{R_p}{R_p + R_{sh} + R_w}, \tag{13}$$

where both R_p and R_{sh} can be obtained by means of the integral of the flux of the Poynting's vector $\mathbf{S}$ in the boundaries of the load and the shielding. Considering normalized fields per Ampère $\bar{\mathbf{E}} = \mathbf{E}/\hat{I}_{coil}$, $\bar{\mathbf{H}} = \mathbf{H}/\hat{I}_{coil}$, resistances can be expressed as follows:

$$R_\alpha = Re\left[\int_{S_\alpha} \left[\left(\bar{\mathbf{E}} \times \bar{\mathbf{H}}^*\right) \cdot \hat{\mathbf{n}}\right] dS_\alpha\right] \qquad \alpha{=}p, sh \tag{14}$$

The resistance of windings R_w can be analytically calculated by means of the ac-loss model of litz wires proposed in several works [27].

The computational model and boundary conditions adopted to evaluate the temperature distribution in the cookware during the induction cooking process is as follows. A contact interaction was activated between the bottom surface of the cookware and the vitroceramic. A heat transfer boundary condition was defined at this lower surface as a consequence of the cookware-glass interaction:

$$-k\frac{\partial T}{\partial n} = h_c(T - T'), \tag{15}$$

where k is the thermal conductivity of the pan or glass, $h_c = 50$ W/(m^2·K) is the contact conductance [10], and T and T' the temperature at the pan and glass surfaces, respectively.

Convective boundary conditions were defined at the outer surface of the pan and the glass. The pan surface was divided into two parts with different film convection coefficients obtained experimentally in previous works [10]: the external surface ($h_c = 75$ W/(m^2·K)) and the internal or cooking surface ($h_c = 9.5$ W/(m^2·K)). Another convection coefficient ($h_c = 75$ W/(m^2·K)) was used to model the heat flux from the vitroceramic. Finally, further heat loss in the pan due to the radiation effect was specified by the Stefan-Boltzmann law:

$$-k\frac{\partial T}{\partial n} = A\hat{\varepsilon}\hat{\sigma}(T^4 - T_a^4), \tag{16}$$

with A being the area, $\hat{\varepsilon} = 1$ the cookware emissivity, $\hat{\sigma}$ the Stefan-Boltzmann constant, and T and T_a the pan and environment temperatures, respectively.

The mesh used in the electromagnetic part is mapped into the heat transfer simulation model. Therefore, the number of mesh elements is identical. Additionally, in this model the solver is configured to perform transient time-domain simulations.

III. ANALYSIS OF THE DIFFERENT COOKWARE BOTTOM ARRANGEMENTS

A. DESCRIPTION OF THE COOKWARE BOTTOM CONFIGURATIONS

Ferromagnetic materials based on iron alloys (ferromagnetic steels) lead to the best performance in terms of the efficiency of induction heating applications and therefore these materials are currently preferred for pan manufacturing. Efficiencies higher than 95% can be achieved with ferromagnetic pans in current coil arrangements [27] whereas non-magnetic metals, such as aluminum or copper, barely achieve 70% efficiency even with expensive coil arrangements, which is unacceptable from the point of view of reliability and cost. On the other hand, the temperature profile obtained with aluminum

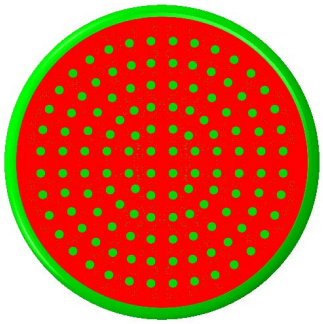

FIGURE 3. Cookware bottom with aluminum inserts.

TABLE 1. Aluminum 3003, steel AISI 304, ferrite and glass ceramic properties.

Symbol, Description [Units]	Alum.	Steel	Ferrite	Glass
ρ, Density [kg/m^3]	2730	7850	4900	2600
k, Thermal conduct. [W/m·K]	190	15	4	2.6
c, Specific heat [J/(kg·K)]	909	500	800	800
$\hat{\sigma}$, Radiation const. [W/m^2 K^4]	0,28	5.1	5.3	5.1
$\hat{\varepsilon}$, Emissivity [-]	0.09	0.8	0.85	0.9
σ_e, Electrical cond. [$(\Omega\cdot m)^{-1}$]	$3 \cdot 10^7$	$8 \cdot 10^6$	5	5
μ_r, Rel. magnetic perm. [-]	1	400-250j	10	1

or copper pans is more uniform due their higher thermal conductivity, and consequently the cooking results are more satisfactory [29].

In this work, in order to balance efficiency against cooking results a solution is proposed based on combining ferromagnetic steel and aluminum. In this arrangement some cylindrical aluminum inserts are place at the cookware's bottom, as it is shown in Fig. 3. Aluminum inserts modify the temperature distribution with respect to a plain ferromagnetic bottom. However, inserts modify the equivalent electrical impedance of the system because some ferromagnetic material is replaced by aluminum.

The properties of the used materials (aluminum, steel, ferrite and glass) are shown in Table 1.

Commercial cookers are connected to the constant-voltage mains, therefore the delivered power depends on factors such as the material of the pot and the pot diameter. The rated power of commercial cookers usually ranges from 2.5 kW to 4 kW for burners of 21 cm diameter.

The temperature of the cookware's bottom depends on the supplied power. Moreover the temperature profile is determined by the planar shape of windings, the distance between the cookware and windings, and the radii of turns. In order to evaluate the performance of the proposed arrangements, a uniformity temperature factor was proposed on the basis of the temperature gradient. This factor was defined as follows:

$$H_t = 1 - \frac{1}{S_p} \int_0^{2\pi} \int_0^{r_{ext}} \frac{\left|\overline{T} - T\,(r,\theta)\right|}{\overline{T}} \cdot r \cdot dr \cdot d\theta \quad (17)$$

where S_p is the bottom surface area, and $\overline{T}$ is the average temperature. This factor ranges between 0 and 1, with 1 representing perfect temperature uniformity.

B. ELECTROMAGNETIC RESULTS

Fig. 4(a) shows the power density per unit of ampere for the homogeneous steel pan. This case illustrates the typical power density generated by a circular planar coil with uniform turn density. As can be observed, power is mainly concentrated in a ring due to the shape of the field generated by circular currents, which is reflected in the temperature profile and is negatively perceived by the users.

Although the transferred power depends on the electromagnetic properties of the material, the aspect of the normalized power density is independent of these properties and cannot be made more uniform by using a single piece of either ferromagnetic or non-ferromagnetic materials. Therefore, as mentioned above, the possibilities provided by inserts in the bottom of the pan were explored. Fig. 4(b) shows the normalized power density per unit of ampere corresponding to case of a bottom with inserts of 8 mm diameter. As can be observed, the power dissipated in the inserts is lower than in the ferromagnetic areas, which helps to mitigate the high-power-density ring observed in Fig. 4(a).

Apart from 8 mm inserts, other diameters were also tested. Table 2 shows electrical parameters at 30 kHz for an aluminum-bodied pan with a steel bottom containing aluminum inserts. As it can be observed, results depend on the number and diameter of inserts, the area covered by them ($A_{inserts}$) and the total pan area (A_{pan}). The impedance changes with the number of inserts, which is reflected in the delivered power. As it is shown, inserts reduce both the power factor and efficiency with respect to the homogeneous case; however, differences between the inserts are small because the area covered is similar for each insert diameter.

TABLE 2. Electrical parameters for the different bottom arrangements.

Parameter		Insert diameter		
	Homogeneous	4 mm	6 mm	8 mm
Number of inserts	-	488	224	128
$A_{inserts}$ / $A_{pan}(\%)$	0	21.51	22.38	22.81
R_{eq} [Ω]	3.25	2.78	2.73	2.71
L_{eq} [μH]	18.19	15.72	14.95	14.07
PF	0.494	0.49	0.50	0.52
η_{ind} (%)	96.13	95.34	95.29	95.24
Max power [W]	3495.4	3021.4	3015.3	2981.4
Uniformity factor H_t	0.78	0.861	0.865	0.87

C. TEMPERATURE RESULTS

Fig. 5 presents the temperature simulated results for the two considered bottom arrangements, the homogeneous bottom and bottom with aluminum inserts. For the sake of clarity, only the case corresponding to 8 mm inserts is represented since the results were very similar to those obtained with 4 and 8 mm inserts. The delivered power and time of the supplied power corresponds to the conditions of the experiments presented in the next section. Some relevant observations can be made. First, the maximum temperatures were similar in both cases. Second, the minimum temperature is higher in the case of the arrangements with aluminum inserts, Fig. 5 (b).

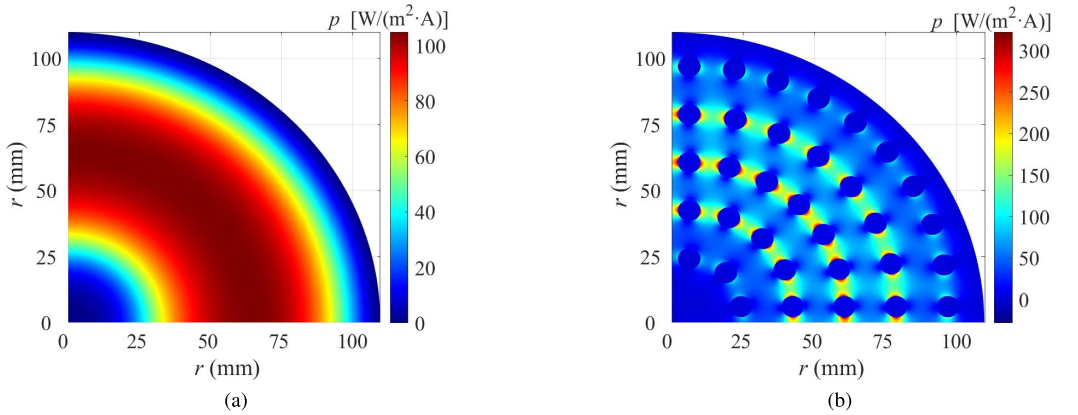

FIGURE 4. Power density per ampere at the bottom of different loads. (a) Homogeneous bottom. (b) bottom with inserts of 8 mm diameter.

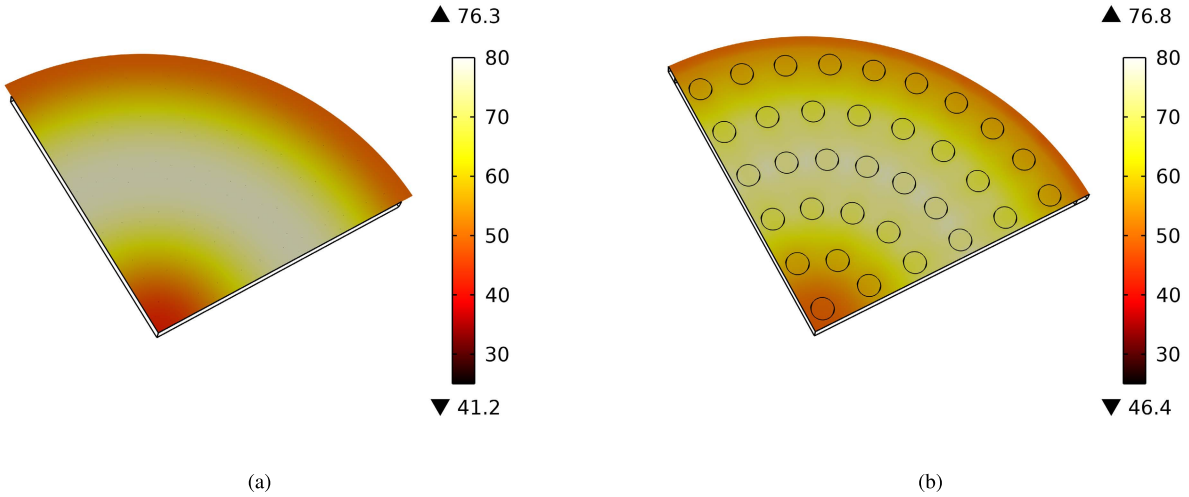

FIGURE 5. Temperature distribution (°C) for different bottom arrangements: (a) homogeneous disk after 30 seconds at 3500 W, (b) bottom with inserts after 35 seconds at 3000 W.

This result suggests that the uniformity of the temperature could be higher than the case of homogeneous bottom.

Regarding the uniformity of the temperature distribution, the values of parameter H_t are shown in Table 2. The homogeneous steel bottom presented the lowest uniformity factor (0.78) and an improvement is observed in the other cases. In any case, this factor is similar for the different diameters of the considered inserts.

IV. EXPERIMENTAL RESULTS

The results previously presented were checked by means of experimental results. For this purpose, an experimental setup was designed partially based on elements of commercial cooktops, and other elements specifically designed to provide some flexibility to the experiments. Commercial elements comprise the inductor system (windings, ferrites and shielding), the vitroceramic and the power electronics converter. Windings consist of a $n = 17$ coplanar turns of $r_{int} = 25$ mm and $r_{ext} = 102.5$ mm internal and external radii, respectively. Windings are made of a litz wire of $n_s = 120$ strands of diameter $\phi_s = 200\mu$m. Windings are fed by a half-bridge series resonant inverter connected to the mains. The power supplied into the load is controlled by means of the inverter switching frequency in the range comprised between 30 kHz and 75 kHz. The operating frequency is set by means of a user interface running in a computer.

Several loads were specifically designed for the verification purpose, having in mind the following aspects: first, the thermal behaviour depends on the bottom configuration rather than the aluminum body, which mainly helps to equalize the temperature. Second, loads should have different $A_{inserts}/A_{pan}$ ratios. Third, in view of the simulation results, where effects were more patent with inserts of diameter 8 mm, only this diameter was considered. Consequently, loads were implemented by means of ferromagnetic disks of 220 mm diameter with detachable inserts, as it is shown in Fig. 6. Inserts were made of both aluminum and the ferromagnetic base material in order to interchange them in different experiments, moreover they were designed in such a way that the surface facing the windings was perfectly

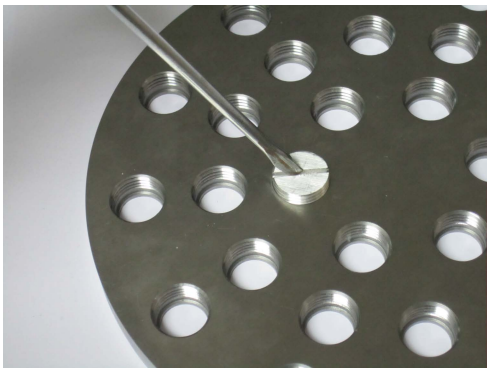

FIGURE 6. Image of the developed loads with detachable inserts.

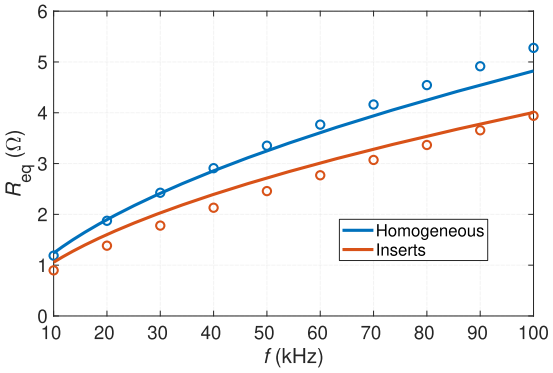

FIGURE 7. Simulated (dots) and measured (line) equivalent resistance R_{eq} for the homogeneous disk and the disk with 128 aluminum inserts.

smooth. Apart from the holed disks, a homogeneous ferromagnetic disk was also built.

First tests were intended to corroborate the electromagnetic model. The impedance of the inductor system with different loads was measured by using the Keysight E4980A LCR meter and the results were compared with simulations. Equivalent resistance and inductance results are shown in Fig. 7 and Fig. 8, respectively. Results include the homogeneous

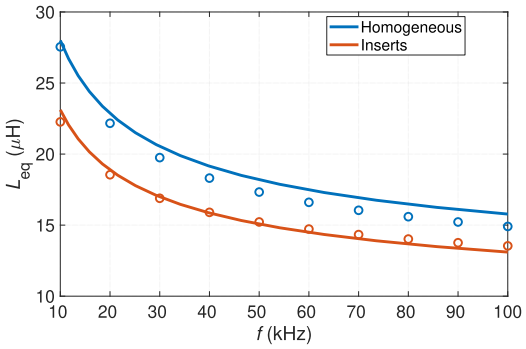

FIGURE 8. Simulated (dots) and measured (line) equivalent inductance L_{eq} for the homogeneous disk and the disk with 128 aluminum inserts.

disk and the disk with aluminum inserts of 8 mm diameter. The equivalent resistance accounts for load, windings and shielding contributions. An acceptable agreement between simulations and measurements is observed at the considered frequency range.

The second set of tests was focused on the thermal behavior of the developed loads. Both disks were heated at the nominal power level, however the power delivered in both cases was slightly different because electronics was connected to the constant voltage mains whereas the equivalent impedance of the disks was different, as it can be observed in Table 2, Fig. 7 and Fig. 8. In any case, the power was applied during short periods of time in order to avoid dangerous temperatures in the setup. Temperature was recorded by means of a FLIR-A655sc infrared camera during the heating process. Infrared cameras have some limitations for temperature measurements, for instance, they are not appropriate for measuring the temperature of a mass of water, due to water behaving as a black body. For this reason, the conditions of simulations and experiments are different from the final use of the cookware, i.e. a cooking process.

In order to check the thermal simulation model, the evolution temperature at the center of the two considered bottom arrangements are presented in Fig. 9. In this case the

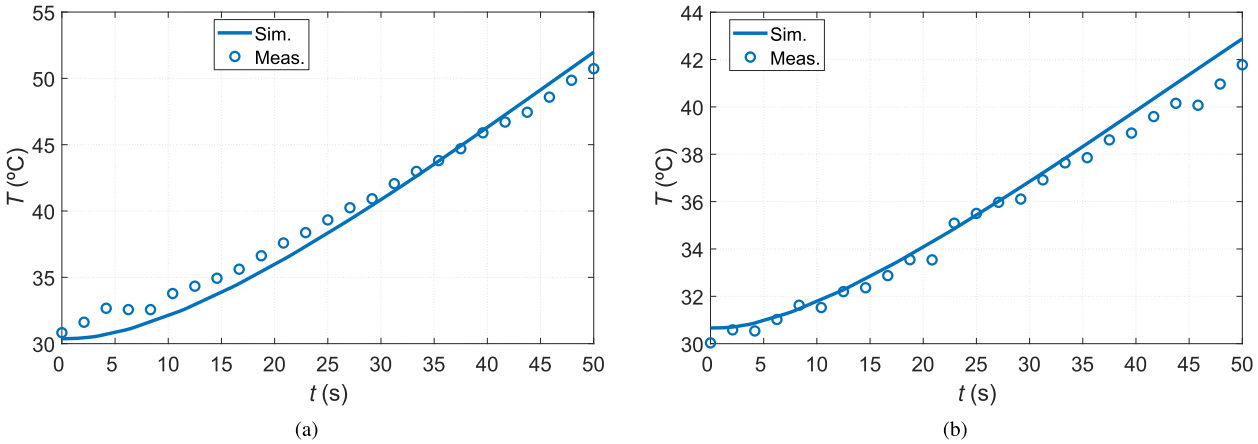

FIGURE 9. Simulated (dots) and measured (line) temperature evolution at the center of the disk heated at the rated power. (a) Homogeneous. (b) Inserts.

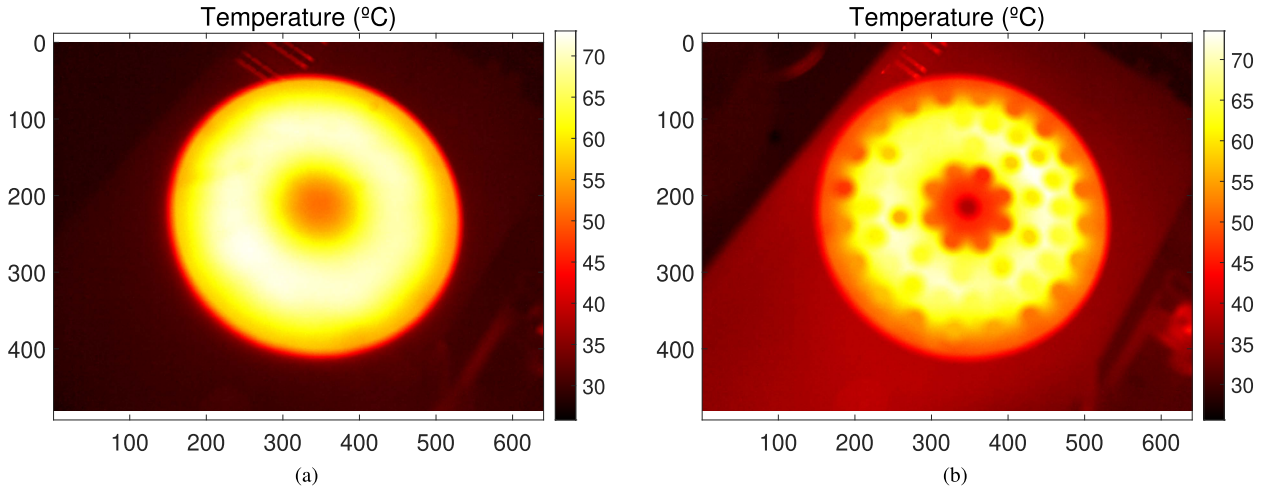

FIGURE 10. Thermographic image of the temperature distribution for different bottom arrangements: (a) homogeneous disk after 30 seconds at 3500 W, (b) bottom with inserts after 35 seconds at 3000 W.

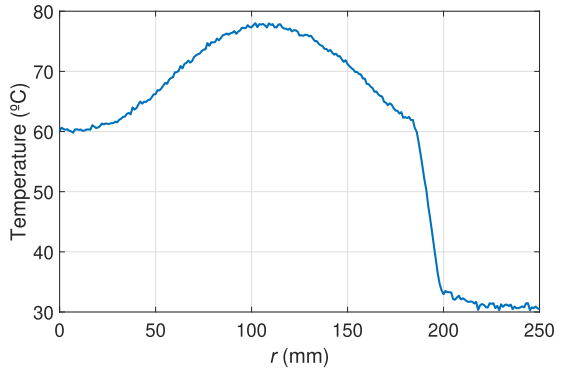

FIGURE 11. Radial temperature profile in the homogeneous disk after 30 seconds at 3500 W.

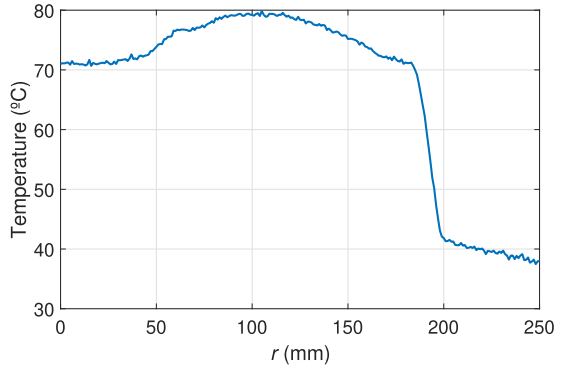

FIGURE 12. Radial temperature profile in the disk with inserts after 35 seconds at 3000 W.

rated power was supplied during 50 seconds. The agreement observed in both cases confirms that the finite element model can be used for further analyses.

Regarding the temperature distribution, experimental results are presented in Fig. 10. As it can be observed, temperature qualitatively follows the temperature distributions of Fig. 5. Regarding the temperature profiles, it is also shown in Fig. 12 that temperature profile is more uniform for the case of the disk with inserts. This is also reflected in the uniformity temperature factor. Simulated and experimental results of the temperature distribution in the surface in contact with the food are compared in Table 3. As it can be observed, experimental values are lower than simulated. The origin of discrepancies lies in the differences between the simulation model and the prototypes. For instance, the contact between the inserts and the cookware base is perfect in simulation, whereas the detachable inserts are screwed into the base of the prototypes. Moreover, properties of materials are constant in simulation but these properties can change with temperature. Additionally, the movement of the air surrounding the prototypes could become turbulent when the temperature increases and this regime mainly can affect the convective heat interchange between the heated piece and the air.

TABLE 3. Comparison between simulated and measured uniformity factor H_t.

	Simulated	Experiment
Homogeneous	0.78	0.644
Inserts	0.87	0.738

V. CONCLUSION

The uniformity of the temperature profile in domestic IH appliances is analyzed in this work and some improvement proposals are presented. The domestic IH process is a multy-physics problem that involves several time and length scales. This multiscale-multiphysics problem is addressed by means of COMSOL Multiphysics finite element tool. This tool is used to evaluate a new arrangement for cookware bottoms consisting of the combination of a ferromagnetic base with aluminum inserts. This solution takes advantage of the benefits of both materials. On the one hand, the ferromagnetic material provides good inductive properties and on the other hand the aluminum provides gigh thermal conductivity. According to the obtained results, inserts reduce the delivered

power by 15% due to the decreased ferromagnetic surface. However, the uniformity factor is increased by the 12%. Therefore, the result is a balanced trade off between inductive properties and thermal characteristics.

REFERENCES

[1] J. Acero, J. Burdío, L. Barragán, D. Navarro, R. Alonso, J. García, F. Monterde, P. Hernández, and S. L. I. Garde, "Domestic induction appliances," *IEEE Ind. Appl. Mag.*, vol. 16, no. 2, pp. 39–47, Mar. 2010.

[2] J. Serrano, I. Lope, J. Acero, J. Burdío, C. Carretero, and R. Alonso, "Design and optimization of small inductors on extra-thin PCB for flexible cooking surfaces," *IEEE Trans. Ind. Appl.*, vol. 53, no. 1, pp. 371–379, Jan. 2017.

[3] E. Plumed, I. Lope, and J. Acero, "Induction heating adaptation of a different-sized load with matching secondary inductor to achieve uniform heating and enhance vertical displacement," *IEEE Trans. Power Electron.*, vol. 36, no. 6, pp. 6929–6942, Jun. 2021.

[4] C. Carretero, R. Alonso, and J. Acero, "Interference emission estimation of domestic induction cookers based on finite-element simulation," *IEEE Trans. Electromagn. Compat.*, vol. 58, no. 4, pp. 993–999, Aug. 2016.

[5] E. Plumed, I. Lope, and J. Acero, "EMI reduction via resonator coils in glassless integrated domestic induction systems," *IEEE Access*, vol. 9, pp. 128147–128156, 2021.

[6] H. Sarnago, O. Lucia, M. Pérez-Tarragona, and J. Burdío, "Dual-output boost resonant full-bridge topology and its modulation strategies for high-performance induction heating applications," *IEEE Trans. Ind. Electron.*, vol. 63, no. 6, pp. 3554–3561, Jun. 2016.

[7] H. Sarnago, P. Guillen, J. M. Burdio, and O. Lucia, "Multiple-output ZVS resonant inverter architecture for flexible induction heating appliances," *IEEE Access*, vol. 7, pp. 157046–157056, 2019.

[8] J. Villa, D. Navarro, A. Domínguez, J. I. Artigas, and L. A. Barragán, "Vessel recognition in induction heating appliances—A deep-learning approach," *IEEE Access*, vol. 9, pp. 16053–16061, 2021.

[9] O. Lucía, D. Navarro, P. Guillén, H. Sarnago, and S. Lucía, "Deep learning-based magnetic coupling detection for advanced induction heating appliances," *IEEE Access*, vol. 7, pp. 181668–181677, 2019.

[10] F. Sanz-Serrano, C. Sagüés, and S. Llorente, "Inverse modeling of pan heating in domestic cookers," *Appl. Thermal Eng.*, vol. 92, pp. 137–148, Jan. 2016.

[11] M.-S. Huang, C.-C. Liao, Z.-F. Li, Z.-R. Shih, and H.-W. Hsueh, "Quantitative design and implementation of an induction cooker for a copper pan," *IEEE Access*, vol. 9, pp. 5105–5118, 2021.

[12] J. H. H. Alwash and S. K. Sultan, "Performance prediction of single-sided induction heating system," *IEEE Trans. Energy Convers.*, vol. 25, no. 4, pp. 1057–1062, Dec. 2010.

[13] Y. Wang, X. Tang, and C. Lee, "A prediction of the acoustical properties of induction cookers based on an FVM–LES-acoustic analogy method," *Appl. Math. Model.*, vol. 35, no. 4, pp. 5040–5050, Apr. 2011.

[14] J. Davies, *Conduction and Induction Heating*. London, U.K.: Peter Peregrinus Ltd, 1990.

[15] F. Dughiero, M. Forzan, S. Lupi, and M. Tasca, "Numerical and experimental analysis of an electro-thermal coupled problem for transverse flux induction heating equipment," *IEEE Trans. Magn.*, vol. 34, no. 5, pp. 3106–3109, Sep. 1998.

[16] F. Dughiero, M. Forzan, C. Pozza, and E. Sieni, "A translational coupled electromagnetic and thermal innovative model for induction welding of tubes," *IEEE Trans. Magn.*, vol. 48, no. 2, pp. 483–486, Feb. 2012.

[17] X. Li, L. Ye, M. Li, and Q. Lv, "Research on temperature and braking performance of water-cooled eddy current retarder," *IEEE Access*, vol. 9, pp. 38991–38998, 2021.

[18] D. Zheng and X. Guo, "Analytical prediction and analysis of electromagnetic-thermal fields in PM eddy current couplings with injected harmonics into magnet shape for torque improvement," *IEEE Access*, vol. 8, pp. 60052–60061, 2020.

[19] X. Yang, Y. Liu, and L. Wang, "An improved analytical model of permanent magnet eddy current magnetic coupler based on electromagnetic-thermal coupling," *IEEE Access*, vol. 8, pp. 95235–95250, 2020.

[20] S. Hansson and M. Fisk, "Simulations and measurements of combined induction heating and extrusion processes," *Finite Elements Anal. Design*, vol. 46, no. 10, pp. 905–915, Oct. 2010.

[21] D. Homberg, Q. Liu, J. Montalvo-Urquizo, D. Nadolski, T. Petzold, A. Schmidt, and A. Schulz, "Simulation of multi-frequency-induction hardening including phase transitions and mechanical effects," *Finite Elements Anal. Design*, vol. 121, pp. 86–100, Nov. 2016.

[22] Ó. Lucía, P. Maussion, E. J. Dede, and J. M. Burdío, "Induction heating technology and its applications: Past developments, current technology, and future challenges," *IEEE Trans. Ind. Electron.*, vol. 61, no. 5, pp. 2509–2520, May 2014.

[23] S. Aranda, C. Diez, P. Hernandez, I. Lope, and E. Moya, "Induction heating unit," European Patent EP2 838 315B1, Jul. 12, 2017.

[24] C. Díez, J. Felices, P. J. Hernández, I. Jaca, I. Moratilla, and M. E. Moya, "Cooking device," European Patent EP3 383 138B1, Mar. 30, 2017.

[25] C. Díez, J. Felices, P. J. Hernández, I. Jaca, I. Moratilla, and M. E. Moya, "Cooking device," European Patent EP3 383 139A1, Mar. 30, 2017.

[26] M. Aoyama, W. Thimm, M. Knoch, and L. Ose, "Proposal and challenge of Halbach array type induction coil for cooktop applications," *IEEE Open J. Ind. Appl.*, vol. 2, pp. 168–177, 2021.

[27] J. Acero, C. Carretero, R. Alonso, and J. M. Burdío, "Quantitative evaluation of induction efficiency in domestic induction heating applications," *IEEE Trans. Magn.*, vol. 49, no. 4, pp. 1382–1389, Apr. 2013.

[28] J. Acero, R. Alonso, J. M. Burdio, L. A. Barragan, and D. Puyal, "Frequency-dependent resistance in litz-wire planar windings for domestic induction heating appliances," *IEEE Trans. Power Electron.*, vol. 21, no. 4, pp. 856–866, Jul. 2006.

[29] F. Sanz Serrano, C. Sagues, and S. Llorente, "Power distribution in coupled multiple-coil inductors for induction heating appliances," *IEEE Trans. Ind. Appl.*, vol. 52, no. 3, pp. 2537–2544, May 2016.

EMILIO PLUMED (Member, IEEE) received the M.Sc. degree in electrical engineering and the Ph.D. degree in power electronics from the University of Zaragoza, Zaragoza, Spain, in 2016 and 2022, respectively. He is currently with the BSH Home Appliances, Zaragoza, where he is involved in several projects focusing on developing domestic induction heating appliances. His current research interests include electromagnetic modeling of inductive coupled contactless energy transfer systems and loss modeling of magnetic devices.

IGNACIO LOPE (Member, IEEE) received the M.Sc. degree in electrical engineering and the Ph.D. degree in power electronics from the University of Zaragoza, Zaragoza, Spain, in 2010 and 2015, respectively. He is currently with the BSH Home Appliances, Zaragoza, where he is involved in several projects focusing on developing domestic induction heating appliances. He is also an Assistant Professor with the Department of Applied Physics, Universidad de Zaragoza. His current research interests include electromagnetic modeling of inductive coupled contactless energy transfer systems and loss modeling of magnetic devices.

JESÚS ACERO (Senior Member, IEEE) received the M.Sc. and Ph.D. degrees in electrical engineering from the University of Zaragoza, Zaragoza, Spain, in 1992 and 2005, respectively. From 1992 to 2000, he worked in several industry projects, especially focused on custom power supplies for Research Laboratories. Since 2000, he has been with the Department of Electronic Engineering and Communications, University of Zaragoza, where he is currently a Professor. His main research interests include resonant converters for induction heating applications, inductive-type load modeling, and electromagnetic modeling. He is a member of the IEEE Power Electronics Society, the IEEE Industrial Electronics Society, and the IEEE Magnetics Society. He is also a member of the Instituto de Investigación en Ingeniería de Aragón (I3A).